High-Stress Optical Birefringence in Pure and Degenerate *n*-Type Germanium*†

ALBERT FELDMAN‡‖
Department of Physics and Institute for the Study of Metals, The University of Chicago, Chicago, Illinois
(Received 2 May 1966)

The stress birefringence in degenerate As- and Sb-doped Ge containing between $N=1.2\times10^{18}$ and 7.2×10^{18} impurities per cc was measured as a function of uniaxial [111] compression at 1.4°K. Wavelengths in the range 1.8–2.5 μ and stresses up to 8×10^{9} dyn/cm^2 were used. These stresses were high enough to cause a transfer of all electrons to a single conduction-band valley, and thus effect a saturation in the birefringence of the free carriers. Deviations of the results from the simple degenerate model are ascribed to tail states below the conduction-band edge and a possible increase of effective mass with N. The birefringence due to interband transitions in As-doped Ge was found to differ by an amount proportional to N from that of pure Ge and also from Sb-doped Ge. The cause for this difference is attributed to the large central-cell potential of As impurities. The stress optical constants of pure Ge were also measured in the above-mentioned wavelength range. Agreement with the data of Schmidt-Tiedemann was found. The stress optical constant for [111] stress Q_{44} shows a linear dependence on the photon energy E at 4.2° and 90°K, while the stress optical constant for [100] stress, $Q_{11}-Q_{12}$, deviates strongly from a linear dependence on E. In addition, the birefringence for [100] stress exhibits a nonlinear stress dependence. The stress birefringence of pure Ge is interpreted in terms of the effect of stress on the electronic transitions in the neighborhood of critical points in the interband density of states.

I. INTRODUCTION

THE stress-induced free-carrier birefringence depends on the effective-mass anisotropy of the carriers. It can therefore be used, particularly in multivalley semiconductors, to study the effect of large impurity concentrations on the shape of the band extrema. We have extended the work of Schmidt-Tiedemann[1] in *n*-type Ge to lower temperatures and to uniaxial stresses high enough to cause a transfer of all carriers to a single valley ([111] stress orientation). The free-carrier birefringence then reaches a saturation value which depends upon the anisotropy of the effective mass of a single conduction-band valley but is independent of the deformation potential and the elastic constants of the material. This work complements the high-stress piezoresistance measurements[2–4] which depend on the mobility components of an individual valley.

It is still uncertain to what degree the presence of a large impurity concentration affects the conduction and valence bands. It is known that the band gaps decrease with increasing carrier concentrations[5,6] and that this effect depends on the type of impurity used.[7] While only a small increase of the electric-susceptibility effective mass with increasing carrier concentration has been observed,[8] indicating a negligible effect of the impurities on the band structure, several anomalies were observed in transport properties of degenerate semiconductors which seem to indicate rather strong deviations of the bands from those of a pure crystal. Thus, tunneling experiments[9] require for their explanation a sizeable number of tail states[10,11] in the forbidden-gap region; resistivity measurements show a temperature dependence[12] well below the degeneracy temperature; anomalous effects have been observed in the magnetoresistance[13] over a wide impurity-concentration range; and impurity-band effects are found even when the impurity activation energy is zero.[3,4] Since transport effects depend both on the effective masses and the relaxation time, it seems important to carry out an experiment which depends only on the effective masses.

High-stress birefringence measurements at 1.4°K were performed on As- and Sb-doped Ge with carrier

* This work was supported by the U. S. Air Force Office of Scientific Research through Grant No. AFOSR 148-63.
† Submitted in partial fulfillment of the requirements for the Ph.D. degree at The University of Chicago.
‡ National Science Foundation Predoctoral Fellow 1962–1964.
‖ Present address: National Bureau of Standards, Washington, D. C.

[1] K. J. Schmidt-Tiedemann, Phys. Rev. Letters **7**, 372 (1961).
[2] H. Fritzsche and M. Cuevas, in *Proceedings of the International Conference on the Physics of Semiconductors, Exeter, 1962* (The Institute of Physics and The Physical Society, London, 1962), p. 29.
[3] M. Cuevas and H. Fritzsche, Phys. Rev. **137**, A1847 (1965).
[4] M. Cuevas and H. Fritzsche, Phys. Rev. **139**, A1628 (1965).
[5] J. I. Pankove, Phys. Rev. Letters **4**, 454 (1960); Ann. Phys. (N.Y.) **6**, 331 (1961); C. Haas, Phys. Rev. **125**, 1965 (1962); J. I. Pankove and P. Aigrain, *ibid.* **126**, 956 (1962); M. Cardona and H. S. Sommers, Jr., *ibid.* **122**, 382 (1961).
[6] A. B. Fowler, W. E. Howard, and G. E. Brock, Phys. Rev. **128**, 1664 (1962).
[7] L. V. Keldysh and G. P. Proshko, Fiz. Tverd. Tela. **5**, 3378 (1963) [English transl.: Soviet Phys.—Solid State **5**, 2481 (1964)].
[8] W. G. Spitzer, F. A. Trumbore, and R. A. Logan, J. Appl. Phys. **32**, 1822 (1961).
[9] R. A. Logan and A. G. Chynoweth, Phys. Rev. **131**, 89 (1963); D. Meyerhofer, G. A. Brown, and H. S. Sommers, Jr., *ibid.* **126**, 1329 (1962).
[10] For references see E. O. Kane, Phys. Rev. **131**, 79 (1963).
[11] J. I. Pankove, in *Progress in Semiconductors*, edited by A. F. Gibson *et al.* (John Wiley & Sons, Inc., New York, 1965), Vol. 9.
[12] S. H. Koenig, in *Proceedings of the International Conference on the Physics of Semiconductors, Exeter, 1962* (The Institute of Physics and The Physical Society, London, 1962), p. 5.
[13] W. Sasaki and Y. Kanai, J. Phys. Soc. Japan **11**, 894 (1956); W. Sasaki, C. Yamanouchi, and G. M. Hatoyama, in *Proceedings of the International Conference on Semiconductor Physics, Prague, 1960* (Academic Press Ltd., London, 1961), p. 159; J. F. Woods and C. Y. Chen, Phys. Rev. **135**, A1462 (1964); W. Sasaki, J. Phys. Soc. Japan **20**, 825 (1965); H. Roth, W. D. Straub, W. Bernard, and J. E. Mulbern, Phys. Rev. Letters **11**, 328 (1963).

concentrations varying from 1.2×10^{18} to 7.2×10^{18} cm^{-3}. The wavelength range was 1.8–2.5 μ. Low temperatures were used so that saturation in the free-carrier birefringence was observed at the lowest possible stress. Uniaxial compressional stresses along [111] of up to 8×10^{9} dyn/cm^2 were used, corresponding to strains of up to about 0.5%. The results are compared to the simple degenerate model.[2] The major deviations are attributed to the presence of tail states below the conduction-band edge. Nonparabolic corrections to the shape of the valleys, which show up as changes of effective mass with carrier concentration are discussed.

The free-carrier birefringence was obtained from the total-stress birefringence by subtracting the interband contribution, which was obtained by measuring the stress birefringence in pure Ge. Although the main interest is in the free-carrier birefringence, a discussion of interband birefringence is also presented. The interband birefringence will be shown to depend on the removal of the degeneracies of the symmetrically related points in the band structure of Ge and the stress dependence of the transition matrix elements.

II. THEORETICAL CONSIDERATIONS

The birefringence of a cubic crystal under uniaxial stress is the phase difference per unit sample thickness between the normal polarization modes of radiation propagating through the crystal. For uniaxial stress applied along a symmetry axis and radiation propagating perpendicular to the stress direction, the birefringence is given by the expression

$$\Delta/t=2\pi(n_{\parallel}-n_{\perp})/\lambda, \tag{1}$$

where λ is the radiation wavelength and $n_{\parallel}$ and $n_{\perp}$ are the refractive indices for polarization parallel and perpendicular to the stress axis, respectively. In a region of the spectrum with little absorption (the extinction coefficient $\ll1$) the birefringence expressed in terms of the principal components of the real part of the dielectric tensor $(\epsilon_1)_{\parallel}$ and $(\epsilon_1)_{\perp}$, and the zero-stress refractive index n_0 is

$$\Delta/t=\pi[(\epsilon_1)_{\parallel}-(\epsilon_1)_{\perp}]/(\lambda n_0). \tag{2}$$

The calculation of the birefringence thus reduces to the calculation of the anisotropy in $\boldsymbol{\varepsilon}_1$ under stress.

The stress-induced change in $\boldsymbol{\varepsilon}_1$ can be expanded as a power series in the stress X which in the low-stress limit is

$$\delta\boldsymbol{\varepsilon}_1=\lambda n_0\mathbf{Q}\cdot\mathbf{X}/\pi, \tag{3}$$

where $\mathbf{Q}$ is a fourth-rank tensor with three independent components called the stress optical constant.[14] Stress is defined to be positive for extension. Thus for X along [111] and [100] one obtains for the birefringence

$$\Delta/t=Q_{44}X \tag{4a}$$

and

$$\Delta/t=(Q_{11}-Q_{12})X, \tag{4b}$$

respectively. In birefringence measurements, Q_{11} and Q_{12} always appear together as $Q_{11}-Q_{12}$. They can be determined individually either by measuring directly $\delta(\epsilon_1)_{\parallel}$ and $\delta(\epsilon_1)_{\perp}$ for [100] stress or by measuring $\delta\boldsymbol{\varepsilon}_1$ under hydrostatic pressure in conjunction with the birefringence measurements.

The birefringence is the sum of interband and free-carrier (intraband or Drude) terms

$$\Delta/t=\Delta^I/t+\Delta^F/t. \tag{5}$$

In the present work we are mainly interested in Δ^F/t.

In the following the free-carrier birefringence in Ge will be computed assuming (1) N electrons in the conduction band which is undistorted by the presence of N donor impurities per cc (simple degenerate model[2]), (2) that the stress merely shifts the conduction-band minima (valleys) without changing their respective effective masses,[15] and (3) that the valleys are parabolic.

One is justified in using the simple degenerate model because the carrier concentrations used here are higher than the critical carrier concentration for the transition from nonmetallic to metallic conduction[16] in Sb- and As-doped Ge. This transition is usually defined as the carrier concentration at which the thermal activation energy of impurity conduction[17] vanishes, which occurs at $N\approx10^{17}$/cc.

The conduction band of Ge has minima (valleys) in the four equivalent [111] directions located at the Brillouin zone edge. The effective-mass components are $m_{\parallel}=(1.588\pm0.005)m_e$ and $m_{\perp}=(0.08152\pm0.00008)m_e$.[18] At zero stress all four valleys are equivalent; hence the expression for the free-carrier dielectric constant for $\omega^2\tau^2\gg1$ is[19]

$$\epsilon_1{}^F=-\frac{4\pi Ne^2}{3\omega^2}\left(\frac{1}{m_{\parallel}}+\frac{2}{m_{\perp}}\right). \tag{6}$$

---

[14] The definition of the stress optical constant $\mathbf{Q}$ is that used by Schmidt-Tiedemann. Nye defines a stress optical constant $\boldsymbol{\pi}$ by the equation

$$\delta\boldsymbol{\varepsilon}^{-1}=\boldsymbol{\pi}\cdot\mathbf{X},$$

where $\mathbf{Q}$ and $\boldsymbol{\pi}$ are related by

$$\mathbf{Q}=-(\pi/\lambda)n_0{}^3\boldsymbol{\pi}.$$

See J. F. Nye, *Physical Properties of Crystals* (Oxford University Press, London, 1957), pp. 243–254.

[15] R. W. Keyes, in *Solid State Physics*, edited by F. Seitz and D. Turnbull (Academic Press Inc., New York, 1960), Vol. 11, p. 167.

[16] N. F. Mott, Phil. Mag. **6**, 287 (1961).

[17] H. Fritzsche, Phys. Chem. Solids **6**, 69 (1958); Phys. Rev. **125**, 1552 (1962).

[18] B. W. Levinger and D. R. Frenkl, J. Phys. Chem. Solids **20**, 281 (1961); G. Dresselhaus, A. F. Kip, and C. Kittel, Phys. Rev. **104**, 368 (1955); R. N. Dexter, H. J. Zeiger, and B. Lax, *ibid.* **104**, 637 (1956).

[19] W. G. Spitzer and H. Y. Fan, Phys. Rev. **106**, 882 (1957).

For uniaxial [100] stress the four valleys remain degenerate in energy, so that no change in ϵ_1^F is expected except for a small effect due to the stress dependence of the effective masses[20] which is neglected in this approximation. For compression along [111], one valley moves down in energy and three move up with a relative energy separation between the lower and upper valleys equal to $4S_{44}\Xi_u X/9$, where S_{44} is the shear component of the elastic-compliance tensor and Ξ_u is the shear deformation potential.[21] There is a net transfer of carriers to the lower valley, giving rise to anisotropy in the dielectric tensor which becomes

$$(\epsilon_1^F)_{ij}=-\frac{4\pi e^2}{\omega^2}\sum_\nu N_\nu\left(\frac{1}{m}\right)_{ij}^\nu, \tag{7}$$

where N_ν is the concentration of carriers and $(m^{-1})_{ij}^\nu$ is the ij component of the reciprocal effective-mass tensor for the νth valley. The general expression for the free-carrier birefringence for [111] stress is then

$$\Delta^F/t=\frac{e^2\lambda}{n_0c^2}\left(\frac{1}{m_\perp}-\frac{1}{m_{11}}\right)(N_L-N_U). \tag{8}$$

The stress dependence enters through N_L and N_U, the concentration of carriers in the lower and each of the upper valleys, respectively; Eq. (8) shows the dependence of Δ^F/t on the effective-mass anisotropy. In the following, the free-carrier birefringence is discussed only in the low-temperature limit [i.e., the zero-stress Fermi level measured from the bottom of the valleys $E_F(0)$ is much larger than kT].

In the high-stress limit one obtains for the saturation value of the free-carrier birefringence

$$\frac{\Delta^F(\text{sat})}{t}=\frac{e^2\lambda N}{n_0c^2}\left(\frac{1}{m_\perp}-\frac{1}{m_{11}}\right). \tag{9}$$

Saturation occurs at the stress

$$X(\text{sat})=-9E_F(0)/(4^{1/3}S_{44}\Xi_u). \tag{10}$$

In the low-stress limit the free-carrier stress optical constant is

$$Q_{44}^F=-\frac{1}{6}\frac{e^2\lambda}{n_0c^2}\left(\frac{1}{m_\perp}-\frac{1}{m_{11}}\right)\frac{S_{44}\Xi_u N}{E_F(0)}. \tag{11}$$

Schmidt-Tiedemann[1] has computed Q_{44}^F for $E_F(0)\ll kT$.

An interesting result of the above calculation is that the curve of $\Delta^F/\lambda Nt$ plotted against $X/E_F(0)$ is independent of λ and N. The proof for this is given in the Appendix.

[20] Cyclotron resonance in uniaxially stressed silicon indicates very small changes in the electron effective mass with stress. See J. C. Hensel, H. Hasegawa, and M. Nakayama, Phys. Rev. **138**, A225 (1965).

[21] The notation used is that of Herring and Vogt [Phys. Rev. **101**, 944 (1956)].

III. EXPERIMENTAL DETAILS

The experiment was performed by passing polarized radiation through stressed Ge. Monochromatic infrared radiation with a resolution of better than 0.01 eV was obtained from a Perkin-Elmer model 210B fore-prism grating monochromator. Wavelengths in the range 1.8–2.5 μ, i.e., photon energies of 0.49–0.69 eV, were used. This wavelength range is a region of minimum absorption for degenerate Ge. The radiation was chopped at 90 cps to permit use of phase-sensitive detection and to eliminate the effects of stray radiation. A pair of Glan-Thompson prisms in a crossed orientation were used as polarizer and analyzer. The sample was placed in a cryostat[22] with Pyrex windows. The radiation was focused over an area of about 0.2×3.0 mm on the sample. A liquid-nitrogen-cooled lead sulfide photoresistor was used as the radiation detector.

The sample preparation has been described previously.[23,24] Samples were aligned by x-ray diffraction to better than 1° and cut to dimensions of approximately 25×1.0×0.6 mm. The carrier concentration N of the degenerate samples (Table I) was determined from Hall-effect measurements on samples cut adjacent to those used in the optical measurements. For a many-valley cubic semiconductor with axially symmetric valleys,[21] N is given in terms of the Hall coefficient R and the mobility anisotropy $K=\mu_\perp/\mu_{11}$ by[8,25]

$$N=3K(K+2)/Re(1+2K)^2, \tag{12}$$

where K was taken to be[3,4] 4.0. The uncertainty in N was ±5%. The pure Ge samples had resistivities greater than 10 Ωcm at 300°K so that the free-carrier effect could be neglected.

TABLE I. Sample characteristics.

Sample	N (cm^{-3})	$E_F(0)$[a] (eV)	E_F(sat)[b] (eV)
As-1	1.24×10^{18}	7.6×10^{-3}	19.1×10^{-3}
As-2	3.12	14.0	35.2
As-3	3.67	15.6	39.3
As-4	4.00	16.6	40.8
As-5	5.45	20.3	45.1
As-6	7.14	24.4	61.5
Sb-1	1.38	8.2	20.6
Sb-2	4.66	18.4	46.3

[a] $E_F(0)$ is zero-stress Fermi level assuming parabolic bands.
[b] E_F(sat) is saturation-stress Fermi level assuming parabolic bands.

The stressing apparatus (Fig. 1) has been described before.[3,24] The stress was changed smoothly by extending the spring with a motor drive. A linear variable differential transformer (LVDT) yielded a signal pro-

[22] The cryostat was built by H. S. Martin and Son.
[23] H. Fritzsche, Phys. Rev. **115**, 336 (1959).
[24] F. Pollak, Phys. Rev. **138**, A618 (1965).
[25] M. Cordona, W. Paul, and H. Brooks, Helv. Phys. Acta **33**, 329 (1960).

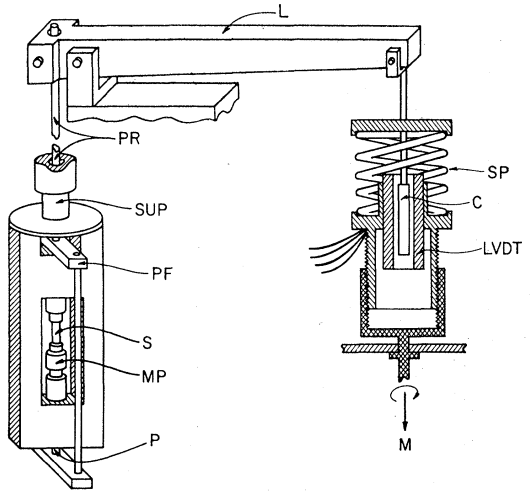

FIG. 1. Stressing apparatus. M=motor drive, LVDT=linear variable differential transformer, C=movable core of LVDT, SP=spring, L=lever arm, PR=pull rod, SUP=supporting member, PF=pulling frame, S=sample, MP=movable piston, P=pin pushing the movable piston upwards.

portional to the extension of the spring. At the start and finish of each stress sweep, the output was calibrated against a matched LVDT mounted on a micrometer head. The samples were carefully mounted into the sample holder with epoxy resin. Exact alignment avoided breakage at high stresses and reduced friction to a minimum. The reproducibility of the data for increasing and decreasing stress indicated that the amount of friction present, and hence the uncertainty in the stress, was always less than 2% of the maximum stress.

The sample was placed between the polarizer and the crossed analyzer. The polarizer was oriented at 45° with respect to the stress axis, so that the components of radiation polarized parallel and perpendicular to the stress axis were of equal intensity. With the stress along a major symmetry axis of the crystal, each polarization component of the radiation propagates through the sample with a different velocity and suffers a different attenuation. The radiation emerging from the sample is thus elliptically polarized. The intensity through the analyzer is given by

$$I=\tfrac{1}{2}I_0(\tfrac{1}{2}(A_{\parallel}+A_{\perp})-(A_{\parallel}A_{\perp})^{1/2}\cos\Delta), \qquad (13)$$

where I_0 is the intensity of radiation incident upon the sample and $\frac{1}{2}I_0A_{\parallel}$ and $\frac{1}{2}I_0A_{\perp}$ are the intensities of the radiation leaving the sample polarized parallel and perpendicular to the stress axis, respectively. The intensity I can be plotted directly as a function of stress X on an X-Y recorder by applying the signal from the infrared detector to the y axis and the signal from the LVDT to the x axis of the recorder. The output intensity for a sample of pure Ge is shown in Fig. 2. The slight damping of the intensity oscillations is caused by the finite bandwidth of the radiation and stress inhomogeneity in the sample. Relative stress gradients smaller than 3%/mm are needed to explain the effect. Figure 3 shows the output intensity for a sample of the As-doped Ge. The envelope of the oscillations for the degenerate sample is caused mainly by stress-induced free-carrier dichroism[26] and impurity gradients in the sample which were found to be less than 0.3×10^{18}/cc/mm. It can be shown that if I' is the height of the intensity curve above the lower envelope, and I_0' the height between the envelopes at the same stress value, then

$$I'=(\tfrac{1}{2}I_0')(1-\cos\Delta). \qquad (14)$$

From this one obtains the birefringence Δ/t as a function of stress.

IV. RESULTS AND DISCUSSION

A. Free-Carrier Birefringence

In Fig. 4 we see Δ/t plotted as a function of [111] compression for pure Ge and As-doped Ge measured at 2.1 μ. Because the birefringence of the pure Ge is linear with stress, it is described by the stress optical constant Q_{44} over the entire stress range. The values of Q_{44} in pure Ge, shown in Table II, are accurate to better than 2%.

Assuming the interband birefringence Δ^I/t in degenerate Ge is equal to the birefringence of pure Ge, one can obtain from Eq. (5) the free-carrier birefringence Δ^F/t as a function of stress. At the highest stresses one obtains an error in Δ^F/t of about 8% in the lowest concentration sample and of about 2% in the highest concentration sample.

Figure 5 shows Δ^F/t for typical samples of As- and Sb-doped Ge as calculated making the above assumption. The horizontal arrows show the values of $\Delta(\text{sat})/t$ calculated from Eq. (9). The stresses at which saturation is expected to occur are shown by the vertical

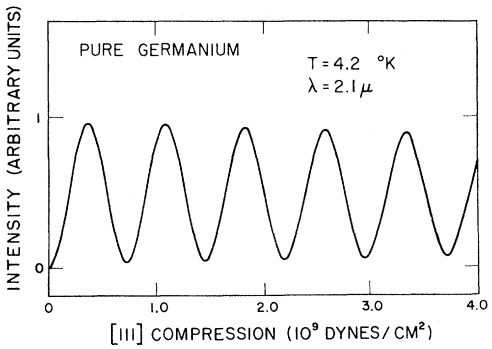

FIG. 2. Intensity as function of stress for a sample of pure Ge.

[26] Free-carrier dichroism is the anisotropy in the free-carrier absorption which is related to the anisotropy in $\varepsilon_2{}^F$, just as the free-carrier birefringence is related to the anisotropy in $\varepsilon_1{}^F$. By measuring I as a function of stress with the polarizers oriented parallel and perpendicular to the stress axis, and taking into account the inhomogeneities mentioned above, the envelope functions have been reproduced.

TABLE II. Stress optical constants in pure Ge in units of deg cm kg^{-1}.

λ (microns)	4.2°K	90°K	300°K	350°K
		Q_{44}		
1.8	6.61[a]	6.66	6.38	6.18
1.9	6.32	6.38	6.33	6.21
2.0	6.04	6.01	6.12	6.05
2.1	5.74	5.76	5.90	5.89
2.2	5.51	5.52	5.68, 5.7±0.2[b]	···
2.4	5.03	5.06	5.27	5.26
2.5	4.83	4.86	5.06	5.08
		$Q_{11}-Q_{12}$		
1.8	0.77	0.62	−1.12	
1.9	···	0.91	−0.40	
2.0	···	1.07	···	
2.1	1.22	1.14	0.41	
2.2	···	1.20	0.63, 0.61±0.05[b]	
2.4	···	1.27	···	
2.5	1.40	1.27	···	

$(1/2)(Q_{11}-Q_{12}+Q_{44})$ Stress [110] Beam [1̄10]

λ (microns)	90°K		300°K	
1.8	3.68[c]	3.64[d]	···	···
1.9	3.64	3.65	3.06[c]	2.97[d]
2.0	3.59	3.54	···	···
2.1	3.54	3.45	3.22	3.16
2.2	3.42	3.36	···	···
2.4	3.21	3.17	···	···
2.5	3.11	3.07	2.99	···

[a] All experimental values have an error of ±0.10 deg cm kg^{-1}.
[b] Obtained by Schmidt-Tiedemann; see Ref. 33.
[c] The data in this column were obtained experimentally.
[d] This column was obtained by averaging Q_{44} and $Q_{11}-Q_{12}$ obtained previously.

arrows. They were computed from Eq. (10) using $S_{44}=1.47\times10^{-12}$ cm^2/dyn and[23] $\Xi_u=19$ eV. The expected saturation of Δ^F/t is observed in the Sb-doped sample. However, the saturation occurs at a higher stress value than expected. This is attributed to tail states below the conduction-band edge. Further evidence for tail states will be discussed later. In all the As-doped samples measured, it was found that Δ^F/t did not saturate but exhibited a linear stress dependence well beyond the stress at which saturation was expected. In their high-stress piezoresistance measurements, Cuevas and Fritzsche also observed saturation in Sb-

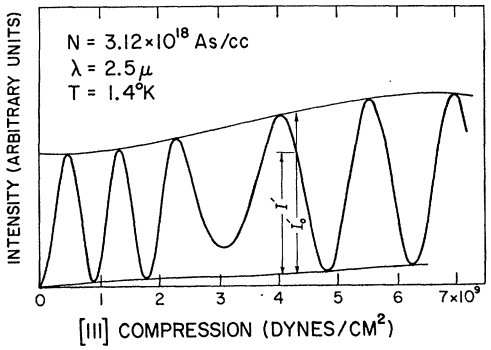

FIG. 3. Intensity as a function of stress for a sample of As-doped Ge.

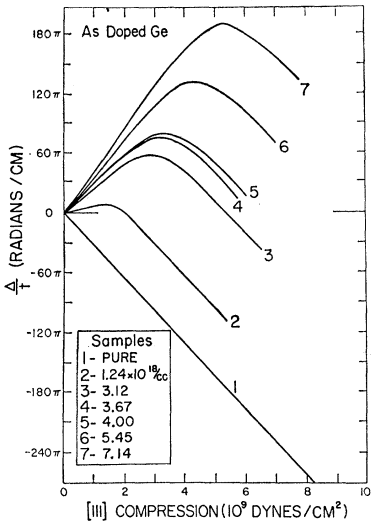

FIG. 4. The birefringence for pure and As-doped Ge as a function of [111] compression at $\lambda=2.1$ μ and $T=1.4$°K.

doped[3] Ge, but not in As-doped[4] Ge. Figure 6 shows that saturation can be achieved in Δ^F/t for As-doped Ge by subtracting a correction factor which is proportional to N from Q_{44} of pure Ge. These correction factors are shown in Table III. In measuring the indirect absorption edge in compensated Sb- and As-doped Ge, Keldysh and Proshko[7] also found a difference due to the different dopants. The indirect edge did not change with Sb concentrations up to 10^{19}/cc while it decreased in energy with increasing As concentrations greater than 10^{18}/cc. In addition, the strength of the absorption at the indirect edge increased with increasing As concentrations. The difference between As and Sb impurities was attributed to the greater effectiveness of As impurities for transmitting momentum in indirect transitions. This results from the much larger central

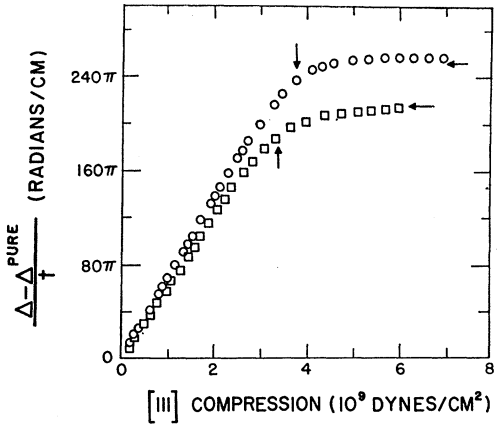

FIG. 5. The birefringence in degenerate Ge minus the birefringence in pure Ge as a function of [111] compression for a sample of Sb- and As-doped Ge. In the Sb-doped sample this is equal to the free-carrier birefringence (see text). The vertical arrows indicate the stress at which saturation is expected and the horizontal arrows indicate the expected saturation values assuming parabolic bands. The temperature is 1.4°K, λ equals 2.1 μ. ○—4.66×10^{18} Sb/cc; □—4.00×10^{18} As/cc.

TABLE III. Corrections to the stress optical constant of pure Ge, Q_{44}, for As-doped Ge at 1.4°K.

λ (μ)	δQ_{44} (10^{-18} deg cm/kg)
1.8	$(-0.10\pm0.03)N$
1.9	$(-0.10\pm0.03)N$
2.1	$(-0.10\pm0.03)N$
2.5	$(-0.07\pm0.03)N$

cell potential of As impurities which accounts for the large chemical shift[27] in the impurity levels of As donors. The additional absorption in As-doped samples might account for the corrections in Q_{44} because it occurs at energies close to the photon energies used in this experiment. In the following, all values of Δ^F/t in As-doped Ge are obtained assuming the above mentioned correction to Q_{44}.

The saturation value of Δ^F/t is plotted in Fig. 7 as a function of N. The errors in $\Delta^F(\text{sat})/t$ are approximately $\pm2\%$. The solid line is a plot of Eq. (9) in which the effective-mass components obtained by cyclotron resonance were used. A small increase in effective mass of the order of magnitude observed by Spitzer *et al.*[8] and Bowers[28] would explain the small deviations of the experimental points from the solid line at the higher carrier concentrations. Alternatively, the deviations might be caused by a change in the mobility anisotropy with N, which would affect the value of N calculated from Eq. (12). The first explanation is supported by the fact that calculations of the nonparabolicity of the conduction-band valleys at the point L in the Brillouin zone yield effective-mass increases of the correct magnitude. From the $\mathbf{k}\cdot\mathbf{p}$ method[29] and a two-band model which neglects spin-orbit splitting, E measured from the bottom of the valley in a direction transverse to [111] is found to be

$$E(k_\perp)=\frac{\hbar^2k_\perp^2}{2m_\perp^0}\left(1-\alpha\frac{\hbar^2k_\perp^2}{2m_\perp^0}\right). \tag{15}$$

Assuming the constant-energy surfaces are ellipsoidal, one obtains for the transverse effective-mass component the term

$$\frac{1}{m_\perp}=\frac{1}{m_\perp^0}(1-9/5\alpha E), \tag{16}$$

which is obtained from the free-carrier electric susceptibility[19]

$$\chi_\perp=-\frac{Ne^2}{m_\perp\omega^2}=-\frac{e^2}{\hbar^2\omega^2}\int\frac{\partial^2E}{\partial k_\perp^2}\frac{2}{(2\pi)^3}f_0d\Omega_k, \tag{17}$$

where f_0 is the occupation probability function and $d\Omega_k$ is the volume element in $\mathbf{k}$ space. The factor α is equal to the reciprocal energy gap at the symmetry point L ($E_L=2.0$ eV)[30] and $m_\perp^0$ is the transverse effective mass at the bottom of the valley. Equation (15) agrees with an orthogonalized-plane-wave (OPW)

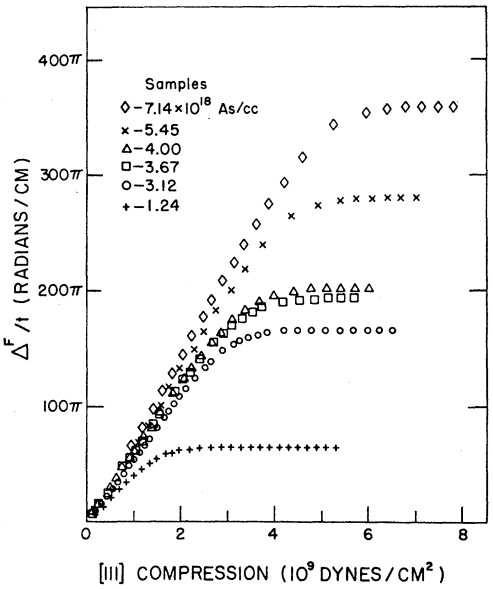

FIG. 6. The free-carrier birefringence as a function of [111] compression for As-doped Ge at $\lambda=2.1$ μ and $T=1.4$°K. A correction to the stress optical constant of pure Ge, which is proportional to the carrier concentration, was applied (see Table III). This results in the saturation of the free-carrier birefringence for all the As-doped samples.

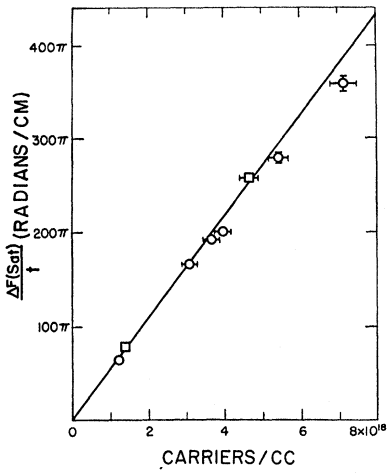

FIG. 7. Saturation value of the free-carrier birefringence as function of carrier concentration taken from measurements at $\lambda=2.1$ μ. The solid line was calculated for parabolic bands. ○—As doping; □—Sb doping.

[27] In phosphorus-doped Ge, where the chemical shift is half way between that in As- and Sb-doped samples [see J. H. Reuszer and P. Fisher, Phys. Rev. **135**, A1125 (1964)], the behavior appears to be the same as that of Sb-doped Ge in the few samples measured.

[28] R. Bowers, Phys. Rev. **108**, 683 (1957).

[29] E. O. Kane, J. Phys. Chem. Solids **1**, 249 (1957).

[30] K. L. Shaklee, F. H. Pollak, and M. Cardona, Phys. Rev. Letters **15**, 883 (1965).

TABLE IV. Selection rules at some critical points in the interband density of states of Ge neglecting spin-orbit coupling.

Transition[a]	Symmetry direction	Energy gap (eV)	Selection rules for matrix elements for given polarization direction
$\Gamma_{25'} \rightarrow \Gamma_{2'}$	[000]	0.8	Allowed for all polarizations
$L_{3'} \rightarrow L_1$	[111]	2.0[b]	Not allowed for [111] Allowed for all directions $\perp$ to [111]
$\Lambda_3 \rightarrow \Lambda_1$	[111]	2.3	Not allowed for [111] Allowed for all directions $\perp$ to [111]
$X_4 \rightarrow X_1$	[100]	4.3	Not allowed for [100] Allowed for all directions $\perp$ to [100]
$\Sigma_4 \rightarrow \Sigma_1$	[110]	4.4	Not allowed for [110] and [$\bar{1}$10] Allowed for [001]

[a] See Ref. 31.
[b] See Ref. 30.

pseudopotential band calculation[31] carried out for the neighborhood of the minima at L. In the two-band model, the $\mathbf{k}\cdot\mathbf{p}$ matrix element for computing $m_{\parallel}$ is zero because of the selection rules listed in Table IV. Thus, $m_{\parallel}$ is expected to change negligibly with energy.

The value of $m_{\perp}^{-1}-m_{\parallel}^{-1}$ obtained from the saturation value of Δ^F/t is plotted against N in Fig. 8. The horizontal line assumes parabolic valleys, while the curved line is obtained using Eq. (16). Both curves assume that the shapes of the valleys are independent of X and N. Because of the relatively large errors due mainly to the $\pm 5\%$ error in the determination of N, one can only state that the present experiments are not in disagreement with the most recent measurements[8] and with the theoretically determined value of the energy dependence of the effective masses. The data demonstrate that the addition of a large number of impurities hardly alters the effective-mass anisotropy of the valleys of pure Ge at the Fermi level.

Figure 9 shows $\Delta^F/\lambda Nt$ versus X for a sample of As-doped Ge at several wavelengths. The fact that the

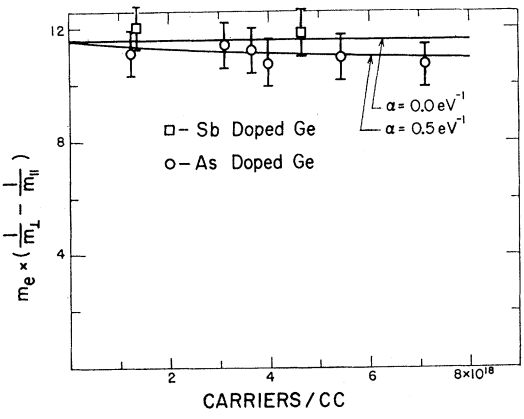

FIG. 8. Reciprocal transverse mass minus reciprocal longitudinal mass as a function of carrier concentration for the conduction band minima of Ge. The upper line is for parabolic bands. The lower line is obtained from a band calculation around the symmetry point L. For clarity the horizontal error bars were omitted. □—Sb-doped Ge; o—As-doped Ge.

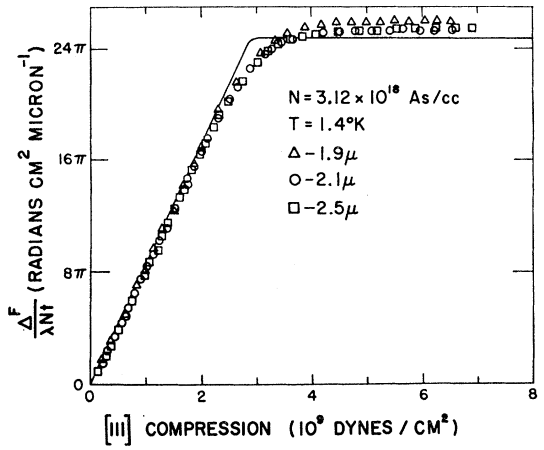

FIG. 9. Free-carrier birefringence, normalized with respect to wavelength and carrier concentration, as a function of [111] compression for a typical sample of As-doped Ge at three wavelengths. The solid curve was calculated using the value for the nonparabolic correction parameter $\alpha = 0.5$ eV^{-1}.

data fall on a single curve demonstrates that Δ^F/t is proportional to λ which implies $\omega^2\tau^2 \gg 1$. All the other samples exhibit the same λ dependence in Δ^F/t. The solid curve was calculated using Eqs. (8) and (16) with $\alpha = 0.5$ eV^{-1}. The value of the deformation potential $\Xi_u = 18$ eV was used so as to obtain the best fit with the data at low stress. The experimental points follow the shape of the theoretical curve except near the onset of saturation, where the discrepancy is attributed to the tailing of states into the forbidden gap of pure Ge.[11] The various causes of tailing have recently been discussed by Pankove.[32] The present experiment indicates that approximately 10–15% of the states occupied by the carriers are tail states and that this percentage is independent of N within the experimental error. A similar percentage can be calculated for GaAs from the results discussed by Pankove.[32] Direct comparison of the present results with optical-absorption data[6] cannot be made, however, because the stress dependence of the tail states is unknown. The data agree with the theoretical curve beyond the onset of saturation within the experimental error which is about $\pm 7\%$ for $\Delta^F(\text{sat})/\lambda Nt$ largely because of the 5% error in N.

The plot of $\Delta^F/\lambda Nt$ against $X/E_F(0)$ at $\lambda = 2.1\ \mu$ for several samples having different carrier concentrations is shown in Fig. 10. Data from all the other samples (except Sb-1 which comes close) fall within the range of the points shown. The solid curve is derived from Eq. (8) assuming parabolic valleys (i.e., $\alpha = 0$). The difference in the shape of the data curves and the theoretical curve in the region near saturation is again attributed to the presence of tail states.

Figures 9 and 10 together demonstrate that $\Delta^F/\lambda Nt$ plotted against $X/E_F(0)$ is independent of λ and N within the experimental error.

[31] After Brust. See David Brust, Phys. Rev. 134, A1337 (1964).

[32] J. I. Pankove, Phys. Rev. 140, A2059 (1965).

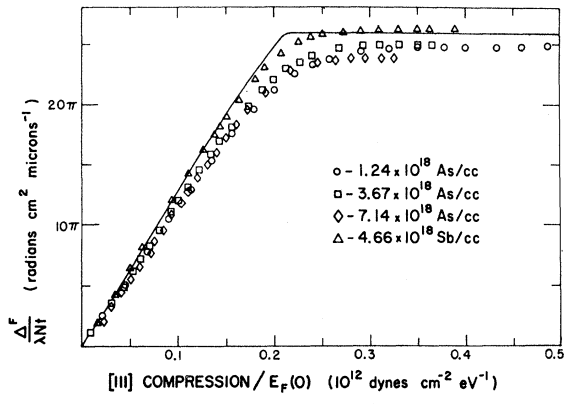

FIG. 10. Free-carrier birefringence, normalized with respect to wavelength and carrier concentration, as a function of [111] compression, normalized with respect to the zero-stress Fermi level, for samples of As- and Sb-doped Ge at $\lambda=2.1$ μ. The solid curve was calculated for parabolic bands.

B. Interband Birefringence in Pure Ge

The measured values of the stress optical constants of pure Ge are given in Table II and plotted in Fig. 11 as a function of photon energy E. There is excellent agreement with the values obtained by Schmidt-Tiedemann.[33] As an experimental check, the stress optical constant for [110] stress and [$\bar{1}$10] beam propagation direction, $Q=\frac{1}{2}(Q_{11}-Q_{12}+Q_{44})$, was measured and found to agree with the average of Q_{44} and $Q_{11}-Q_{12}$ measured separately, within the experimental error. There are two main features to notice about the data plotted in Fig. 11. First, it is found that $Q_{44}\gg Q_{11}-Q_{12}$. Second, it is noticed the Q_{44} shows a linear E dependence at 4.2° and 90°K and only small deviations from linearity at higher temperatures. On the other hand, $Q_{11}-Q_{12}$ deviates strongly from a linear E dependence.

In the following we attempt to understand the interband birefringence in pure Ge which, in the present case, is related to $\delta\varepsilon_1(X)$, the change in ε_1 with stress, because the extinction coefficient is very small. The Kramers-Kronig dispersion relations relate $\delta\varepsilon_1(X)$ at one photon energy to the change in the imaginary part of the dielectric tensor $\delta\varepsilon_2(X)$ at all energies and hence the interband birefringence at one energy to the stress dependence of the interband transitions at all energies.

In order to compute ε_1 at photon energies far from the region of absorption, Stern[34] approximated the structure in $\varepsilon_2(E)$ as the sum of delta functions each representing transitions associated with a certain volume in $\mathbf{k}$ space. In this case, ε_1 can be written as

$$\varepsilon_1=1+\sum_s \frac{\mathbf{G}^s}{E_s^2-E^2}, \tag{18}$$

where the tensor $\mathbf{G}^s$ is proportional to the oscillator strength of the transition and E_s is the transition energy.

[33] K. J. Schmidt-Tiedemann, J. Appl. Phys. **32**, 2058 (1961).
[34] Frank Stern, Phys. Rev. **133**, A1653 (1964).

Peaks in $\delta\varepsilon_2(X)$ occur at critical points in the interband density of states,[35] therefore, for the purpose of calculating the birefringence we can assume the above sum is over the critical points. The critical points in the interband density of states represent maxima, minima, and saddle points in the dependence of the direct interband energy gap on $\mathbf{k}$.[31] The expression for $\delta\varepsilon_1(X)$ will then depend on the lifting of the degeneracies of symmetrically related critical points and the stress dependence of their transition matrix elements which are contained in $\mathbf{G}^s$.

Because the critical points occur predominantly at symmetry points and along symmetry lines,[36] the contributions to the birefringence due to the lifting of the degeneracies will depend strongly on the stress direction. Thus, contributions from L and Λ critical points vanish for [100] stress while the contributions from Δ and X critical points vanish for [111] stress. In addition, the matrix elements at the critical points have large polarization dependences which result from the selection rules at these points. The selection rules for matrix elements at the most important critical points[37] in Ge

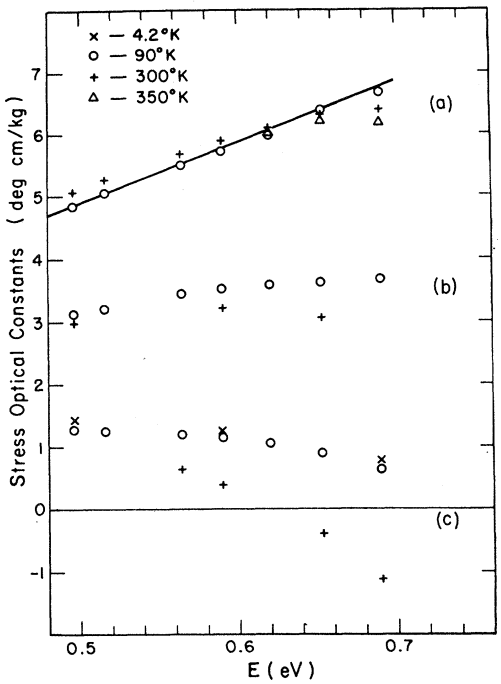

FIG. 11. The stress optical constants of pure Ge as a function of photon energy. (a) Q_{44}. The data at 4.2 and 90°K coincide, within the experimental error. The heavy solid line passes through the origin of the coordinate system. It demonstrates that Q_{44} at 4.2 and 90°K is proportional to the photon energy, within the experimental error. (b) $\frac{1}{2}(Q_{11}-Q_{12}+Q_{44})$. (c) $Q_{11}-Q_{12}$.

[35] G. W. Gobeli and E. O. Kane, Phys. Rev. Letters **15**, 142 (1965); W. E. Engler, M. Garfinkel, and J. J. Tiemann, *ibid.* **16**, 239 (1966).
[36] J. C. Phillips, Phys. Rev. **104**, 1263 (1956).
[37] D. Brust, J. C. Phillips, and F. Bassani, Phys. Rev. Letters **9**, 94 (1962).

TABLE V. The contribution at low photon energies to $\epsilon_{11}-\epsilon_{1}$ due only to the lifting of the degeneracies of some critical points in the interband density of states neglecting spin-orbit splitting.

Critical point[a]	[111] Stress[b,c]	[100] Stress[b,c]
L	$(8/9)(G_1^L/E_L^3)\Xi_u(L)S_{44}X$	0
Λ	$(16/9)(G_1^\Lambda/E_\Lambda^3)\Xi_u(\Lambda)S_{44}X$	0
X	0	$2(G_1^X/E_x^3)\Xi_u(X)(S_{11}-S_{12})X$
Σ	0	$4(G_1^\Sigma/E_\Sigma^3)[3\Xi_p(\Sigma)-4\Xi_u(\Sigma)](S_{11}-S_{12})X$

[a] From Table IV.
[b] The symbols Ξ_u and Ξ_p are the difference between the respective deformation potentials of the conduction and valence bands. The notation is that of Ref. 21.
[c] The components G_1^s are the only nonvanishing components of $\mathbf{G}^s$ in the coordinate system in which $\mathbf{G}^s$ is diagonal. See text for definition of symbols.

are shown in Table IV. Here the small effects of spin-orbit coupling are neglected. These selection rules enable one to determine the sign of the various contributions to the birefringence caused by the lifting of the degeneracies. Table V shows some of these contributions to the birefringence at photon energies much less than the transition energies. For the moment we neglect the Γ transitions. The L and Λ terms dominate the birefringence for [111] stress. The signs of all the constants are positive, in agreement with the observed birefringence. The X and Σ terms dominate the birefringence for [100] stress. By considering the energy denominators alone, we can understand the large size of Q_{44} compared to $Q_{11}-Q_{12}$. It is most likely that the various components G_1^s are approximately of the same size since the matrix elements are not very $\mathbf{k}$-dependent.[31] For this same reason it is probable that the contribution to the birefringence of the stress dependence of the matrix elements is small compared to the contributions because of the lifting of degeneracies.

The magnitude and sign of the stress-induced changes of the matrix elements have not yet been determined. Symmetry arguments do not predict that these contributions to the birefringence will vanish for certain stress directions as was the case of the contributions due to the energy shifts of the critical points.

Although the absorption due to the Γ transitions is weak,[38] the Γ transitions could make a significant contribution to $\mathbf{Q}$ because of their proximity to the energy region of interest. From Eq. (18) it can be seen that at energies much less than the minimum absorption energy $\boldsymbol{\varepsilon}_1$ is independent of E or λ so that $\mathbf{Q}$ is proportional to the photon energy E. The magnitude of the deviation of $\mathbf{Q}$ from a linear E dependence might indicate the size of the contribution from the Γ transitions. Thus $Q_{11}-Q_{12}$ probably contains a large contribution from Γ while Q_{44} does not. The increasing deviations of Q_{44} from a linear E dependence with increasing temperature is caused by the shrinking of the band gap at Γ which brings the Γ transition closer to the photon energies used in the experiment.

Because the relative influence of the Γ transitions on the birefringence for [100] stress is large, these transitions might also be responsible for the nonlinear stress dependence observed in the birefringence for [100] stress which is shown in Fig. 12. These transitions are more complicated than the previous cases because of the degeneracy of the valence bands at Γ. The uniaxial stress lifts the degeneracy[39] and causes the valence bands to split linearly[40] with stress into two highly anisotropic bands. It further causes a mixing of the wave functions resulting in a large stress dependence in the transition matrix elements. Thus the contribution to the birefringence due to Γ is expected to have large nonlinear terms in its stress dependence.

Nonlinear effects have been observed by Gerhardt[41] due to the shift with stress of the Λ saddle points in $\mathbf{k}$ space. The above-mentioned nonlinear effects might be present in the birefringence for [111] stress but have not been observed because of the predominance of the large linear stress effect.

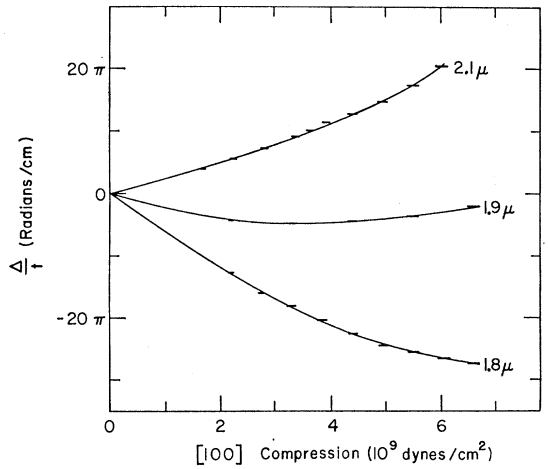

FIG. 12. The birefringence of pure Ge as a function of [100] compression at 300°K.

[38] H. R. Phillip and E. A. Taft, Phys. Rev. 113, 1002 (1959).

[39] W. H. Kleiner and L. M. Roth, Phys. Rev. Letters 2, 334 (1959); G. E. Pikus and G. L. Bir, Fiz. Tverd. Tela 1, 1642 (1959) [English transl.: Soviet Phys.—Solid State 1, 1502 (1960)]; J. J. Hall, Phys. Rev. 128, 68 (1962).
[40] A. M. Glass, Can. J. Phys. 43, 12 (1965).
[41] U. Gerhardt, Phys. Status Solidi 11, 801 (1965).

V. SUMMARY

The free-carrier birefringence measurements on degenerate n-type Ge agree with the simple degenerate model except near the onset of saturation. Here the measurements require for their explanation a tailing of states into the forbidden gap.

A possible increase of effective mass with carrier concentration has been observed, which is consistent with the calculated shape of the valleys of pure Ge. The value for the nonparabolic correction factor α obtained from experiment is $\alpha=0.5\pm0.5$ eV^{-1}. From the energy gap at[30] $L(2.0$ eV) one obtains $\alpha=0.50$ eV^{-1}.

A difference between the stress optical constant Q_{44} in pure Ge and the interband stress optical constant Q_{44}^I in As-doped Ge was found which is proportional to the impurity concentration N. This difference is attributed to the decrease of the energy gaps with N which is related to the large central cell potential of As impurities. The effect has not been observed in Sb-doped Ge where the central cell potential of Sb impurities is much smaller.

The interband birefringence was shown to depend mainly on the direct interband transitions around the critical points in the interband density of states, with those transitions closest to the energy of the measurements having the greatest influence. The stress optical constants of Ge for [111] stress Q_{44} and [100] stress $Q_{11}-Q_{12}$ were measured in the wavelength range 1.8–2.5 μ. It was found that $Q_{44}\gg Q_{11}-Q_{12}$. This was interpreted as being due to the selection rules for transitions at L and Λ. These selection rules cause important contributions to the birefringence to vanish for [100] stress. The Γ transitions were found to have a small relative influence on Q_{44} but a large relative influence on $Q_{11}-Q_{12}$. This was used to explain the nonlinear stress dependence observed in the birefringence for [100] stress.

ACKNOWLEDGMENTS

I wish to thank Professor H. Fritzsche for his encouragement, guidance, and invaluable suggestions throughout all phases of this work. I would like to thank M. Cuevas and F. Mueller for many useful discussions. I would also like to thank B. Miller for the samples of pure germanium. The bulk of the arsenic doped samples were supplied by the General Diode Corporation. The use of the facilities of the Low Temperature Laboratories of The University of Chicago supported by the National Science Foundation is gratefully acknowledged.

APPENDIX

We show here that for aribtrary uniaxial stress, $\Delta^F/\lambda Nt$ versus $X/E_F(0)$ at $T=0$ is independent of λ and N if the assumptions of Sec. II are made. From Eqs. (2) and (7) one can easily show that $\Delta^F/\lambda Nt$ is independent of λ. If suffices then to show that $(\epsilon_1^F)_{ij}/N$ versus $X/E_F(0)$ is independent of N. From Eq. (7) we see that this is implied if N_ν/N versus $X/E_F(0)$ is independent of N.

The shift in energy of the minimum of the νth valley with stress is $\alpha_\nu X$, where α_ν is related to the stress direction, the orientation of the valley, the elastic compliance tensor, and the deformation potentials. If the Fermi level $E_F(X)$ for stress X is measured from the zero-stress position of the valley minima and $E_F(\nu)$ is the Fermi level measured from the minimum of the νth valley, then we obtain for the case of n-type Ge

$$4E_F^{3/2}(0)=\sum_\nu E_F^{3/2}(\nu)=\sum_\nu (E_F(X)-\alpha_\nu X)^{3/2}, \quad \text{(A1)}$$

since $N=\sum N_\nu$. Setting $E_F(X)/E_F(0)=\beta$ we obtain from Eq. (A1)

$$\sum_\nu [\beta-(\alpha_\nu X/E_F(0))]^{3/2}=4. \quad \text{(A2)}$$

Also

$$N_\nu/N=[\beta-(\alpha_\nu X/E_F(0))]^{3/2}. \quad \text{(A3)}$$

In the above, terms corresponding to an empty valley are set equal to zero. By eliminating β from Eqs. (A2) and (A3), we obtain N_ν/N as a function of $X/E_F(0)$ and independent of N. This completes the proof.